

1 **Revision_1**

2 **A neutron diffraction study of boussingaultite,**
3 **(NH₄)₂[Mg(H₂O)₆](SO₄)₂**

4 G. Diego Gatta, Giorgio Guastella, Alessandro Guastoni, Valentina Gagliardi,
5 Laura Cañadillas-Delgado and Maria Teresa Fernandez-Diaz
6

7 **Running title:** Crystal chemistry of boussingaultite

8
9 **Abstract, Keywords**

10 **Introduction**

11 **Sample description and occurrence**

12 **Experimental methods and Results**

- 13 1) Gravimetric determination of sulphates
- 14 2) EDTA titrimetric determination of magnesium
- 15 3) Determination of fluorine and chlorine by ion selective electrode
- 16 4) Determination of water content by heating
- 17 5) Determination of minor elements by inductively coupled plasma atomic
18 emission spectroscopy (ICP-AES) and air-acetylene flame atomic emission
19 spectrometry (FAES)
 - 20 5.1) *Determination of REE concentration by ICP-AES*
 - 21 5.2) *Determination of other minor elements concentration by ICP-AES*
- 22 6) Indirect gravimetric determination of ammonium as (NH₄,Rb,Cs,K)
23 tetraphenylborate
- 24 7) Determination of CHN
- 25 8) Single-crystal neutron diffraction
 - 26 8.1) *Neutron data collections and treatments*
 - 27 8.2) *Neutron structure refinements*

28 **Discussion and implications**

29 **Acknowledgements**

30 **References**

31 **Figures/Tables**

32
33
34 **Corresponding author: G. Diego GATTA**

35 Dipartimento di Scienze della Terra, Università degli Studi di Milano

36 Via Botticelli 23, I-20133 Milano, Italy

37 Tel. +39 02 503 15607, Fax +39 02 503 15597, E-Mail: diego.gatta@unimi.it

38
39
40
41 *Manuscript submitted to American Mineralogist*

A neutron diffraction study of boussingaultite, (NH₄)₂[Mg(H₂O)₆](SO₄)₂

G. Diego Gatta¹, Giorgio Guastella², Alessandro Guastoni³, Valentina Gagliardi⁴,
Laura Cañadillas-Delgado⁵ and Maria Teresa Fernandez-Diaz⁶

¹Dipartimento di Scienze della Terra, Università degli Studi di Milano,
Via Botticelli 23, I-20133 Milano, Italy

²Agenzia delle Accise, Dogane e Monopoli, DTI – Lombardia, Ufficio Antifrode - Sezione Laboratori,
Via Marco Bruto 14, I-20138 Milano, Italy

³Dipartimento di Geoscienze, Università degli Studi di Padova,
Via G. Gradenigo 6, I-35131, Padova, Italy

⁴Istituto Gemmologico Italiano, Piazza San Sepolcro 1, I-20123 Milano, Italy

⁵Institut Laue-Langevin, 71 Avenue des Martyrs, F-38000 Grenoble, France

Abstract

The crystal structure and the chemical composition of boussingaultite from Pécs-Vasas, Mecsek Mountains, South Hungary, were investigated by single-crystal neutron diffraction (at 20 K) along with a series of chemical analytical techniques (*i.e.*, gravimetric determination of sulphates, EDTA titrimetric determination of magnesium, ion selective electrode for F and Cl, indirect gravimetric determination of ammonium as (NH₄,Rb,Cs,K) tetraphenylborate, inductively coupled plasma atomic emission spectroscopy for REE and other minor elements, elemental analysis for C, N and H content, high-*T* mass loss for H₂O content). The concentration of more than 50 elements was measured. The experimental formula of the boussingaultite of this study is: [(NH₄)_{1.77}K_{0.22}]_{Σ1.99}[(Mg_{0.95}Mn_{0.06})_{Σ1.01}(H₂O)_{5.7}](SO₄)_{1.99}. The neutron refinement confirms that the structure of boussingaultite is built up by: isolated Mg(H₂O)₆-octahedra, along with isolated NH₄- and SO₄-tetrahedra connected by a complex H-bonds network. Mg²⁺ is completely solvated by H₂O molecules, in a typical octahedral bonding configuration. All the seven independent oxygen sites of the structure are involved in H-bonds, as *donors* or as *acceptors*. The geometry of all the H₂O molecules, bonded to Mg, is in line with what usually observed in crystalline compounds. The H₂O molecules show moderate-strong H-bonds, with *H...O_{acceptor}* and *O_{donor}...O_{acceptor}* ranging between 1.72-1.87 Å and 2.70-2.84 Å, respectively, along with *O_{donor}-H...O_{acceptor}* angles between 168-178°. The four independent *N-H...O* bonds show *H...O_{acceptor}* and *N_{donor}...O_{acceptor}* distances ranging between 1.81-2.00 and 2.84-2.98 Å, respectively, with *N-H...O* angles between 158-176°. All the H-bonds of the H₂O molecules and of the NH₄-group involve the oxygen sites of the SO₄-group as *acceptors*: the SO₄-group is, therefore, the “bridging unit” between the NH₄ and the Mg(H₂O)₆ units, *via* H-bonds. The structure refinement of this study proved, unambiguously, that the partial K⁺ vs. NH₄⁺ replacement

79 generates a local disorder. K lies at the *N* site, and its bonding configuration is described with a
80 distorted polyhedron with CN=8. However, the K^+ vs. NH_4^+ replacement implies a change in the
81 configuration of the SO_4 -tetrahedron, through a sort of rotation of the polyhedron. This is the first
82 evidence of a partial picromerite component in the boussingaultite structure, which gives rise to a local
83 disorder likely due to the significantly different bonding configurations of the two cations. The
84 refinement proved also that Mn^{2+} replaces Mg^{2+} at the *Mg* site. No evidence of distortion of the
85 octahedron is observed in response to such a replacement, but the fraction of Mn^{2+} is modest. An
86 analysis of previous Raman and IR findings is provided, compared with the experimental results of this
87 study.

88

89 **Keywords:** Boussingaultite, sulphates, neutron diffraction, crystal chemistry, hydrogen bonding.

90

91 **Introduction**

92 Boussingaultite is a magnesium ammonium sulphate hexahydrate, with ideal chemical formula
93 usually given as $(NH_4)_2Mg(SO_4)_2 \cdot 6H_2O$. It is a rare mineral, which occurs as sublimate formed under
94 fumarolic conditions, geysers, or from coal gas at burning coal-dumps (*e.g.*, Cipriani 1959; Larsen and
95 Shannon 1920; Shimobayashi et al. 2011). It is found as stalactites and incrustations, more rarely as
96 monoclinic crystals (short prismatic [001] with {001} prominent). Boussingaultite is one of a wide
97 number of isomorphous compounds (mainly synthetic) called “Tutton’s salts” (Tutton 1900, 1905), a
98 family of double salts with the formula $A^+{}_2B^{2+}(SO_4)_2(H_2O)_6$ (sulphates) or $A^+{}_2B^{2+}(SeO_4)_2(H_2O)_6$
99 (selenates), with A^+ : K, Rb, Cs, Tl or NH_4 , B^{2+} : Mg, V, Cr, Mn, Fe, Co, Ni, Cu, Zn or Cd. Focusing on
100 natural compounds, boussingaultite belongs to the picromerite group of minerals, with picromerite
101 ($K_2Mg(SO_4)_2 \cdot 6H_2O$), nickelpicromerite ($K_2Ni(SO_4)_2 \cdot 6H_2O$), nickelboussingaultite
102 ($(NH_4)_2Ni(SO_4)_2 \cdot 6H_2O$), mohrite ($(NH_4)_2Fe(SO_4)_2 \cdot 6H_2O$), katerinopoulosite ($(NH_4)_2Zn(SO_4)_2 \cdot 6H_2O$),
103 and cyanochroite ($K_2Cu(SO_4)_2 \cdot 6H_2O$). Tutton’s salts structure is monoclinic, usually described in the
104 space group $P2_1/a$ with $a \sim 9.0-9.4$, $b \sim 12.3-12.9$, $c \sim 6.0-6.4$ Å and $\beta \sim 104-107^\circ$, $Z = 2$. The first general
105 structure model was reported by Hofmann (1931), followed by a series of re-investigations for any
106 specific compound of the family based on X-ray or even neutron diffraction, on single-crystal or
107 polycrystalline sample. Concerning boussingaultite, a few crystallographic studies were performed but
108 all on the synthetic counterpart with ideal composition (Margulis and Templeton 1962; Montgomery
109 and Lingafelter 1964; Maslen et al. 1988). As a matter of fact, all the mineralogical databases refer
110 only to the structural models of the synthetic analogous. The building units of the boussingaultite
111 structure consist of isolated $Mg(H_2O)_6$ -octahedra, NH_4 - and SO_4 -tetrahedra connected by a network of

112 H-bonds, which must plays a fundamental role on the stability of the crystalline edifice. In this light,
113 the chemical formula of boussingaultite is better written as $(\text{NH}_4)_2[\text{Mg}(\text{H}_2\text{O})_6](\text{SO}_4)_2$, rather than
114 $(\text{NH}_4)_2\text{Mg}(\text{SO}_4)_2 \cdot 6\text{H}_2\text{O}$ as commonly reported. The presence of NH_4 -group generates a different
115 bonding configuration with respect to other members of the picromerite group, in which *e.g.* K^+
116 replaces NH_4^+ (Bosi et al. 2009). A thorough comparative crystal-chemical study of a series of
117 synthetic compounds with general formula $\text{K}_2[\text{B}^{2+}(\text{H}_2\text{O})_6](\text{SO}_4)_2$, with $\text{B}^{2+} = \text{Mg}, \text{Fe}, \text{Co}, \text{Ni}, \text{Cu}$, and
118 Zn , was reported by Bosi et al. (2009).

119 An additional limitation of the literature data on (natural) boussingaultite concerns the chemical
120 composition of this mineral based on modern standards. Only a few chemical analyses are available,
121 and the reference one is often that reported by Larsen and Shannon (1920) (with wt.% oxide equals to
122 98.3 wt%).

123 There is a raising interest on boussingaultite, or its synthetic counterpart, generated by some
124 potential industrial and agricultural utilization of this material, following the operational principles of
125 circular economy for sustainable development. For example, the global demand for agricultural
126 fertilizer by nutrient from the quaternary system $(\text{NH}_4)_2\text{SO}_4\text{-MgSO}_4\text{-K}_2\text{SO}_4\text{-H}_2\text{O}$ is increasing
127 drastically (*e.g.*, the world capacity for producing ammonia + phosphoric acid + potash increased from
128 292 Mt on 2016 to 316 Mt on 2021; F.A.O. 2019). This leads to the requirement of the new technology
129 for producing an increasing mass of fertilizers: soluble crystalline precipitates (among those,
130 boussingaultite) from industrial waste sludge, as null by-product of polymers manufacturing digested
131 to retrieve the rubber by using sulphuric acid, are used as source of S, N, K and Mg (*e.g.*, Taweepreda
132 2013; Li et al. 2020). A null by-product becomes a second raw material. In addition, boussingaultite
133 (along with other Tutton's salt) is one of the potential materials suitable for strong energy absorption
134 by solar collectors: energy required for domestic heating and hot-water supply could be "stored" in
135 reversible transformations, *e.g.* in chemical reactions or in phase transitions (*e.g.*, Gronvold and
136 Meisingset 1982; Lim and Lee 2010). Salt hydrates, and among those even Tutton's salts, have
137 relatively low dehydration or melting temperatures, representing some among the most promising
138 materials for this purpose. Furthermore, Highfield et al. (2012) reported the role of boussingaultite in
139 the activation of serpentine for CO_2 mineralization by flux extraction of soluble magnesium salts using
140 ammonium sulphate.

141 Considering the capacity of the Tutton's salt structure to allocate a series of cations at the A^+
142 and B^{2+} site, and the presence in nature of isomorphic minerals of boussingaultite in which Mg^{2+} is
143 replaced by Ni^{2+} (*e.g.*, nickelboussingaultite) or in which NH_4^+ is replaced by K^+ (*e.g.*, picromerite),
144 the aim of this study is a reinvestigation of the crystal chemistry of a natural boussingaultite (from

145 Pécs-Vasas, South Hungary) on the basis of a multi-methodological approach based on single-crystal
146 neutron diffraction and a series of chemical analytical techniques in order: *a*) to unveil potential
147 replacement mechanisms at the A^+ and B^{2+} occurring in nature and not described so far, and *b*) to
148 describe unambiguously the location and the anisotropic displacement regime of the proton sites, the
149 geometry of the NH_4 -group along with the complex H-bonding configuration in the structure of
150 boussingaultite.

151

152 **Sample description and occurrence**

153 The sample of boussingaultite used for this study belongs to the mineral collection of the
154 Museum of Mineralogy of the University of Padova (catalogue number MM6606). The hand
155 specimen is made by an aggregate of whitish, colourless, platy-tabular millimetric crystals collected
156 at Pécs-Vasas, Mecsek Mountains, South Hungary (Szakáll and Kristály 2008). Pécs-Vasas is an
157 abandoned coalmine with a large open pit located near Köves Hill. Coal ores of Jurassic age occur
158 within sandstones, claystones, mudstone sedimentary layers and carbonatic rocks. Pécs-Vasas
159 coalfields is the type locality for ammoniomagnesiovoltaite $[(\text{NH}_4)_2\text{Mg}^{2+}_5\text{Fe}^{3+}_3\text{Al}(\text{SO}_4)_{12}\cdot 18\text{H}_2\text{O}]$,
160 Szakáll et al. 2012] and kollerite $[(\text{NH}_4)_2\text{Fe}^{3+}(\text{SO}_3)_2(\text{OH})\cdot \text{H}_2\text{O}]$, Ende et al. 2021). Several others
161 NH_4 , Al, Fe, Mg, Ca and Fe-bearing sulphates were found in the coal dumps of Pécs-Vasas. Most
162 of them occur as euhedral, idiomorphic millimetric crystals, formed by the spontaneous burning and
163 combustion of coal. The most interesting and uncommon NH_4 -bearing sulphate minerals, at this
164 locality, are ammonioalunite and adranosite (Szabó et al. 2015), ammoniojarosite, clairite,
165 efremovite, godovikovite, koktaite, mascagnite, mohrite and tschermigite (Szakáll and Kristály
166 2008). Ammonium sulphates are often accompanied by other more common sulphates, such as
167 alunogen, butlerite, halotrichite, pickeringite, copiapite, gypsum, hexahydrite, kieserite, metavoltine
168 and voltaite. The formation of a relevant number of N-bearing sulphates and sulphites can be
169 explained by the decay of the organic matter of coal, which also contain abundant pyrite and
170 marcasite. These iron sulphides are the source of sulphur oxides, from which sulphates are formed.

171

172 **Experimental methods and Results**

173

174 **1) Gravimetric determination of sulphates**

175 A mass of 150-200 mg of sample was placed in a 400 ml beaker; then, 200 ml of water and
176 1 ml of concentrated hydrochloric acid were added. The clear solution was heated to boiling and 10
177 ml of 10% barium chloride solution was then added dropwise. The beaker was covered with a

178 clockglass and was heated below the boiling point for 4 hours. The precipitate was then filtered and
179 washed with 150 ml of hot water. A filter was placed in a pre-weighted platinum capsule (m1) and
180 dried at 105°C for 1 hour. The filter was then completely incinerated on a Bunsen burner, and the
181 platinum capsule was heated at 800°C until a constant weight (m2) was measured. The different of
182 weigh (m2 - m1) is the total SO₃ content of the mineral, expressed as BaSO₄. The measured fraction
183 of SO₃ was 44.2(2) wt%.

184

185 **2) EDTA titrimetric determination of magnesium**

186 A mass of 100-150 mg of sample were placed in a 200 ml beaker, and then diluted to 100 ml
187 with water. After complete dissolution, 10 ml of buffer solution (pH 10 mix ammonium
188 chloride/ammonia) were added, along with 5 ml of hydroxylammonium chloride (3% solution), 1
189 ml of ammonium sulphide (20% solution) and 3-4 drops of *Eriochrome black-T* solution (2gr/l in
190 ethanol). The solution was then titrated with standard solution of EDTA
191 (ethylenediaminetetraacetic acid) 0.01 M. The end point was reached when the reddish purple
192 colour of the solution altered to blue or green. The total volume of the added EDTA is proportional
193 to the average content of magnesium in the mineral. The measured fraction of MgO was 10.6(2)
194 wt%.

195

196 **3) Determination of fluorine and chlorine by ion selective electrode**

197 A mass of 20 mg of sample was placed in a 50 ml plastic test tube, along with 15 ml of
198 water and 0.5 ml of nitric acid 1M. 2-3 ml of total ionic strength adjustment buffer (*TISAB III*
199 solution) were added to the clear solution, and then diluted to 20 ml with water. Fluorine content
200 was determined using the *perfectION* Combination Fluoride Ion Selective Electrode (by *Mettler*
201 *Toledo*), adopting the conventional method of standard addition. Solutions of fluorine from 0.1 to
202 5.0 mg/l were prepared by Certified Reference Material - CRM 1000 mg/l of fluorine. The resulting
203 F fraction was < 0.01 wt% (uncertainty not determined).

204 A mass of 40 mg of sample was placed in a 50 ml plastic test tube, along with 15 ml of
205 water and 0.5 ml of nitric acid 1M. 2-3 ml of ionic strength adjustment solution (*perfectION ISA*
206 *solid state ISE*) were added to the clear solution, then diluted to 20 ml with water. Chlorine content
207 was determined using the *perfectION* Combination Chloride Ion Selective Electrode (by *Mettler*
208 *Toledo*), adopting the conventional method of standard addition. Solutions of chlorine from 2 to 10
209 mg/l were prepared by CRM 1000 mg/l of chlorine. The resulting Cl fraction was < 0.1 wt%
210 (uncertainty not determined).

211

212 **4) Determination of water content by heating**

213 A mass of 400-500 mg of sample was placed in a quartz crucible with lid and gradually
214 heated (10°C/min) in a muffle furnace from ambient temperature up to 200°C. Assuming that the
215 mass loss represents the total amount of H₂O, the estimated H₂O fraction of the boussingaultite
216 sample was 28.4(2) wt%.

217

218

219 **5) Determination of minor elements by inductively coupled plasma atomic emission** 220 **spectroscopy (ICP-AES) and air-acetylene flame atomic emission spectrometry** 221 **(FAES)**

222 All determinations (excluding caesium) were performed in axial view mode for REE, and
223 radial view mode for the other minor elements, with a *Perkin Elmer Optima 7000DV* ICP-AES
224 spectrometer. Caesium concentration was measured with a *Varian SpectrAA 220FS* air-acetylene
225 flame atomic emission spectrometer.

226

227 **5.1) Determination of REE concentration by ICP-AES**

228 A mass of 50 mg of boussingaultite was placed in a 50 ml volumetric flask, along with 25
229 ml of water and 5 ml of nitric acid 1M. The resulting clear solution was then diluted with water. A
230 calibration protocol was performed with a blank solution and a series of *ad hoc* solutions with REE
231 concentration from 0.001 to 0.050 mg/l for each element (using CRM multi elemental standard mix
232 for ICP). Results and instrumental parameters are listed in Table 1.

233

234 **5.2) Determination of other minor elements concentration by ICP-AES**

235 The determination of the non-REE minor elements was performed using two different
236 protocols, the second one devoted only to the Cs concentration, described below:

237 *i)* 5-100 mg of sample was placed in a 50 ml volumetric flask, 25 ml of water, 5 ml of nitric
238 acid 1M and 5 ml of scandium solution 100 mg/l were added. The resulting clear solution
239 was diluted with water. A calibration protocol was performed with a blank solution and a
240 series of *ad hoc* solutions with concentration from 0.001 to 0.050 mg/l for each element
241 (using CRM multi elemental standard mix for ICP). Results and instrumental parameters
242 are listed in Table 2.

243 ii) A mass of 100-200 mg of sample was placed in a 50 ml volumetric flask, along with 25
244 ml of water, 5 ml of nitric acid 1M and 300 mg of potassium nitrate. The clear solution was
245 then diluted with water. A calibration protocol was performed with a blank solution and a
246 series of *ad hoc* solutions prepared with CRM multi elemental standard mix for ICP,
247 containing 100 mg/l of Cs (5 solutions from 1 mg/l to 20 mg/l). Results and instrumental
248 parameters are listed in Table 2.

249

250 **6) Indirect gravimetric determination of ammonium as (NH₄,Rb,Cs,K)** 251 **tetraphenylborate**

252 A mass of 100-150 mg of boussingaultite was placed in a 200 ml beaker and diluted to 50
253 ml with water. After complete dissolution, 4 ml of 1M hydrochloric acid were added. Then, 8 ml of
254 5% sodium tetraphenylborate solution were slowly added to the solution (in about 5 minutes). After
255 1 hour, the white precipitate was collected on a preweight 30 ml sintered-glass filtering crucible
256 (m1) (porosity n. 4), washed 3 times with 3 ml of 0.1% sodium tetraphenylborate solution and 2
257 times with 2 ml of water. The crucible was dried at 105°C until a constant weight (m2) was
258 measured (about 24 hours). The different of weight (m2 - m1) is the total of (K,NH₄,Rb,Cs) content
259 of the sample expressed as (K,NH₄,Rb,Cs)[B(C₆H₅)₄]. As the fraction of K, Rb and Cs was already
260 known, the fraction of (NH₄)₂O was calculated to be 12.7(3) wt% (Table 3).

261

262 **7) Determination of CHN**

263 Analysis of total carbon, hydrogen and nitrogen was performed using the *Leco CHN*
264 *Truspec* analyser. Carbon was not detectable. Total hydrogen fraction was found to be in
265 accordance, at a first approximation, with ammonium and water fraction of the mineral (*i.e.*, ~5.13
266 wt%). Unsatisfactory results were obtained for nitrogen with this method.

267

268 A representative chemical composition of boussingaultite from Pécs-Vasas is given in Table 3, and
269 its experimental chemical formula is: [(NH₄)_{1.77}K_{0.22}]_{Σ1.99}[(Mg_{0.95}Mn_{0.06})_{Σ1.01}(H₂O)_{5.7}](SO₄)_{1.99}.

270

271

272 **8) Single-crystal neutron diffraction**

273 8.1) *Neutron data collections and treatments*

274 In order to check the quality of the crystals to be used for the neutron diffraction
275 experiments, a series of preliminary tests were performed by single-crystal X-ray diffraction with a
276 Rigaku XtaLABSynergy-i diffractometer, equipped with a PhotonJet-i MoK α microfocus source
277 and a HyPix-6000HE Hybrid Photon Counting (HPC) detector, at the Earth Science Dept. Univ.
278 Milan.

279 A single crystal with size 3.5 x 2.1 x 1.6 mm³ was mounted on a vanadium pin of 1 mm of
280 diameter and placed on a close-circuit displax device on the monochromatic four-circle
281 diffractometer D19 at ILL (Grenoble, France). Neutron diffraction data were collected at 20(1) K,
282 with a wavelength of 0.9500 Å, provided by a flat Cu monochromator using the 331 reflection, at
283 $2\theta_M = 69.91^\circ$ take-off angle (Gatta et al. 2021a). The measurement strategy consisted on several ω
284 scans with steps of 0.07° at different χ and ϕ positions. These ω scans cover either 79° or 64°
285 depending on the χ angle, in order to avoid collisions with the cryostat. *NOMAD* control software
286 from ILL was used for data collection. The unit-cell determination was done by using the *PFIND*
287 and *DIRAX* programs; processing of the raw data, to obtain the integrated intensities, was performed
288 using the *RETREAT* and *RAFD19* programs (McIntyre and Stansfield 1988; Wilkinson et al. 1988;
289 Duisenberg 1992). Absorption effects, due to the low-*T* device and to the crystal size and
290 composition, were corrected using the *DI9ABS* program (Matthewman et al. 1982). The lattice was
291 found to be metrically monoclinic (Table 4, *deposited*), and consistent with the previous
292 experimental findings of boussingaultite reported in the literature. The reflection conditions were
293 found to be consistent with the space group $P2_1/a$. A total number of 8640 reflections were
294 collected (with $-14 \leq h \leq +16$, $-17 \leq k \leq +21$ and $-11 \leq l \leq +5$), out of which 3785 were unique (R_{int}
295 = 0.0371, Laue class $2/m$) and 3463 with $F_o > 4\sigma(F_o)$, with $d_{\text{min}} \sim 0.54$ Å (Table 4, *deposited*). The
296 Wilson plot and the statistics of distributions of the normalized structure factors suggested the
297 structure is centrosymmetric at $\sim 96\%$ likelihood (with the Sheldrick's $|E^2 - 1|$ criterion of 0.981).
298 Further details pertaining to neutron data collection are listed in Table 4 (*deposited*).

299

300 8.2) *Neutron structure refinements*

301 Anisotropic structure refinement, based on the neutron intensity data collected at 20 K, was
302 performed using the SHELXL-2018/3 software (Sheldrick 2015) in the space group $P2_1/a$, starting
303 from the structure model of Montgomery and Lingafelter (1964), without any H atom. Neutron
304 scattering lengths of Mg, Mn, K, S, N, O and H were taken from Sears (1986). Secondary isotropic

305 extinction effect was corrected according to the formalism of Larson (1967), implemented in
306 SHELX; however, the correction was found to be not significant. On the basis of the chemical
307 analysis, the *Mg* site in the structure model of Montgomery and Lingafelter (1964) was modelled as
308 partially occupied by Mg and Mn, and the fraction of the two elements was refined. After the first
309 cycles of refinement, a series of negative residual peaks in the final difference-Fourier map of the
310 nuclear density were found. These negative residual peaks were then assigned to ten independent H
311 sites (*H1*, ..., *H10*) in the next cycles, as H has a negative neutron scattering length. With such a
312 structure model, convergence was achieved and the variance-covariance matrix showed no
313 significant correlation among the refined variables. However, two significant residual peaks were
314 found in the difference-Fourier map of the nuclear density function, only ~0.4 Å apart from the *O1*
315 (*i.e.*, +4.3 fm/Å³) and *O2* (*i.e.*, +3.4 fm/Å³) sites and, in addition, the *N* site required a partial site
316 occupancy for a better figure of merit. The structural model was then adjusted considering; 1) two
317 additional O sites, labelled as *O1A* and *O2A*, with partial and refinable site occupancy, and 2) the *N*
318 site as populated by N and K (according to the chemical analysis), and the fraction of the two
319 elements was refined (fixing $s.o.f.(N)=s.o.f.(H1,H2,H3,H4)$, Table 5 - *deposited*). With this new
320 model, convergence was rapidly achieved and no significant correlation among the refined variables
321 was observed in the variance-covariance matrix. The final residuals were -1.3/+0.8 fm/Å³. All the
322 principal mean-square atomic displacement parameters were positive (excluding the *O1A* and *O2A*,
323 having partial site occupancy, which were modelled as isotropic) and the final $R_1(F)=0.0334$, for
324 3466obs./190par. Additional details pertaining to the structure refinements with and without the
325 split *O1A* and *O2A* sites are listed in Tables 4 (*deposited*), and the relative atomic coordinates and
326 displacement parameters are given in Tables 5, 6 and 7 (*all deposited*) and in the CIFs. Some
327 selected interatomic distances and angles are listed in Table 8.

328

329

330 **Discussion and implications**

331 The chemical data of the boussingaultite from Pécs-Vasas, obtained by the multi-
332 methodological approach of this study, confirm the general chemical formula for this mineral
333 reported in the literature: (NH₄)₂[Mg(H₂O)₆](SO₄)₂. However, two important substituents were
334 detected: Mn²⁺ and K⁺ (Table 2). The crystallographic data confirm that Mn²⁺ replaces Mg²⁺ at the
335 octahedral *Mg* site, whereas K⁺ replaces the NH₄⁺ group (with K lying at the *N* site), giving the
336 actual chemical formula: [(NH₄)_{1.77}K_{0.22}]_{Σ1.99}[(Mg_{0.95}Mn_{0.06})_{Σ1.01}(H₂O)_{5.7}](SO₄)_{1.99} (Table 3). The
337 very low fraction of rubidium (*i.e.*, Rb₂O 0.05 wt%, Table 2) can replace NH₄⁺ along with K⁺, that

338 of iron (*i.e.*, Fe₂O₃ 0.01 wt%, Table 2) can replace Mg at the octahedral *Mg* site. There is no
339 evidence of potential substituents for the SO₄²⁻-group. Silicon (*i.e.*, SiO₂ 0.04 wt%, Table 2) is
340 likely the effect of a low fraction of quartz coexisting with boussingaultite. The concentration of
341 REE and other minor elements is substantially irrelevant (Tables 1 and 2). The protocol here used
342 for the chemical analyses, and for the recalculation of the chemical formula, proved to be
343 appropriate for such a chemically complex materials containing NH₄⁺ and H₂O, which cannot be
344 characterised using the routine protocols in mineralogy, based essentially on EPMA-WDS. We have
345 successfully applied a similar protocol to investigate hydrous minerals containing other light
346 elements as principal constituents, as Li, Be and B (*e.g.*, Gatta et al. 2014, 2019, 2020; Lotti et al.
347 2018). We cannot exclude that the slightly lower fraction of measured H₂O m.p.f.u. with respect to
348 the ideal ones (*i.e.*, 5.7 vs. 6.0 m.p.f.u.) is the effect of a partial dehydration of the starting material,
349 which is not surprising if we consider the occurrence of boussingaultite. However, the potential
350 dehydration was not revealed by the single-crystal neutron structure refinement (based on data
351 collected at 20 K, Table 5).

352 The structure model of boussingaultite obtained in this study, based on neutron diffraction
353 data, is (partially) consistent with that of synthetic (NH₄)₂[Mg(H₂O)₆](SO₄)₂ previously reported by
354 Margulis and Templeton (1962), Montgomery and Lingafelter (1964) and Maslen et al. (1988). The
355 structure consist of three building units: isolated Mg(H₂O)₆-octahedra, along with isolated NH₄- and
356 SO₄-tetrahedra connected by a complex H-bonds network (Fig. 1). Mg²⁺ is completely solvated by
357 H₂O molecules, in a typical octahedral bonding configuration. The geometry of the Mg(H₂O)₆-
358 octahedron is almost ideal, with *Mg-O* distances ranging between ~2.058 and ~2.094 Å, and *O-Mg-O*
359 angles between ~88.70 and ~91.30°. Even the SO₄-tetrahedron is only slightly distorted, having *S-O*
360 distances ranging between ~1.48 and ~1.49 Å and *O-S-O* between ~108.3 and ~110.1°. Isolated SO₄-
361 tetrahedra, connected by H-bonds, usually show such an almost ideal configuration, especially at low
362 temperature (*e.g.*, in thaumasite or in ettringite, Gatta et al. 2012, 2019). The NH₄-tetrahedron shows a
363 modest distortion, with N-H distances and H-N-H angles ranging, respectively, between ~1.024-1.033
364 Å and ~106.5-111.6°. The analysis of the principal root-mean-square components of the atomic
365 displacement parameters show that even the H sites display only a modest anisotropy: the
366 RMS_{\max}/RMS_{\min} ratio is lower than 1.8 for all the seven independent *H* sites (Fig. 1, Table 7 -
367 *deposited*). Furthermore, the H sites of the NH₄-group show a slightly higher libration anisotropy if
368 compared to those of the H₂O molecules (Table 7 - *deposited*).

369 All the seven independent oxygen sites of the structure (*i.e.*, O1, ..., O7, Table 5 - *deposited*) are
370 involved in H-bonds, as *donors* or as *acceptors* (Table 8). The geometry of all the H₂O molecules,

371 bonded to Mg, is in line with what usually observed in crystalline compounds, in which the molecules
372 are involved in H-bonds (*e.g.*, Steiner 1998): the *O-H* distances, corrected for riding motion effect
373 (according to Busing and Levy 1964), range between 0.996 and 1.001 Å, the *H-O-H* angles between
374 105.5 and 108.2° (Table 8). The H₂O molecules show moderate-strong H-bonds, with *H...O_{acceptor}* and
375 *O_{donor}...O_{acceptor}* ranging between 1.72-1.87 Å and 2.70-2.84 Å, respectively, along with *O_{donor}-*
376 *H...O_{acceptor}* angles between 168-178° (Fig. 2, Table 8). All the H-bonds of the H₂O molecules involve
377 the oxygen sites of the SO₄-group as *acceptors* (*i.e.*, *O1*, *O2*, *O3* and *O4*; Fig. 2, Table 8). The longest
378 *H...O_{acceptor}* and *O_{donor}...O_{acceptor}* distances are those with *O5* as *donor* and *O4* as *acceptor* (*i.e.*,
379 *O5...O4* = 2.836(1) and *H6...O4* = 1.870(1)), likely because *O4* is the *acceptor* of three independent
380 H-bonds: *O5...O4*, *O6...O4* and *N...O4* (Table 8). The four independent *N-H...O* bonds show
381 *H...O_{acceptor}* and *N_{donor}...O_{acceptor}* distances ranging between 1.81-2.00 and 2.84-2.98 Å, respectively,
382 with *N-H...O* angles between 158-176° (Table 8). All the H-bonds of the NH₄-group involve the
383 oxygen sites of the SO₄-group as *acceptors* (*i.e.*, *O1*, *O3* and *O4*; Fig. 2, Table 8). The SO₄-group is,
384 therefore, the “bridging unit” between the NH₄ and the Mg(H₂O)₆ units, *via* H-bonds (Fig. 2, Table 8).
385 Each of the *O-H...O* and *N-O...H* bonds involve one *donor* and one *acceptor* only; in other words,
386 there is no evidence of bifurcated (or even trifurcated) H-bonds as found in other hydrous minerals
387 (*e.g.*, Gatta et al. 2011, 2013, 2021b). However, some of the oxygen sites act as *donors* for more than
388 one H-bond: this is the case of the *O1* site (*i.e.*, *N-H2...O1*, *N-H3...O1*, *O7-H10...O1*), of the *O3* site
389 (*i.e.*, *N-H4...O3*, *O5-H5...O3*, *O7-H9...O3*), and of the *O4* site (*i.e.*, *N-H1...O4*, *O5-H6...O4*, *O6-*
390 *H8...O4*) (Fig. 2, Table 8). Overall, the H-bonding network in boussingaultite is complex and
391 pervasive, and the structure stability is expected to be substantially governed by that. This can
392 explain previous experimental findings on the isomorphous (NH₄)₂[Fe(H₂O)₆](SO₄)₂,
393 (NH₄)₂[Zn(H₂O)₆](SO₄)₂ or (NH₄)₂[Co(H₂O)₆](SO₄)₂ that showed, by *in-situ* high-temperature
394 experiments (*i.e.*, ¹H and ¹⁴N NMR, TG, DSC) the structural collapse at relatively low temperature:
395 320-360 K (Lim 2012; Park and Lim 2017).

396 The structure refinement of this study proved, unambiguously, that the partial K⁺ vs. NH₄⁺
397 replacement generate a local disorder. K lies at the *N* site, and its bonding configuration is that reported
398 in Table 5 (*deposited*), describing a distorted polyhedron with CN=8 (*K-O_{min}* ~ 2.60 and *K-O_{max}* ~ 3.23
399 Å). However, the K⁺ vs. NH₄⁺ replacement implies a change in the configuration of the SO₄
400 tetrahedron, through a sort of rotation of the polyhedron about the *O3-O4* vector: the *O3* and *O4* sites
401 are kept, whereas the *O1* and *O2* sites are replaced respectively by the *O1A* and *O2A* sites, only ~0.4 Å
402 from the parental ones, as shown in Fig. 1. Whereas the *O1A* and *O2A* are well detectable, this is not
403 the case for the position of the *S* site of the “rotated” tetrahedron, so that only the external geometry of

404 the rotated tetrahedron is described in Table 5 (*deposited*). The refined fraction of K^+ is 0.26 a.p.f.u.,
405 slightly higher than that obtained by chemical analysis (*i.e.*, 0.22 a.p.f.u., Table 3). To the best of our
406 knowledge, this is the first evidence of a partial picromerite component in the boussingaultite
407 structure, which gives rise to a local disorder likely due to the significantly different bonding
408 configurations of the two cations. However, the disorder does not generate any significant effect at the
409 lattice level, as shown by the fully indexed diffraction pattern. Can the data reported in this study
410 corroborate a potential boussingaultite-picromerite solid solution? It is not possible to answer
411 unambiguously to this question, which requires more data with different compositions along the
412 join. However, this study is the first step toward a better understanding of the substitution
413 mechanisms in natural NH_4 -bearing Tutton's salts. The refinement proved also that Mn^{2+} replaces
414 Mg^{2+} at the *Mg* site. No evidence of distortion of the octahedron is observed in response to such a
415 replacement, but the fraction of Mn^{2+} is modest. The refined fraction of Mn^{2+} is virtually identical to
416 that obtained by the chemical analysis, *i.e.*, 0.06 a.p.f.u. (Tables 3 and 5-*deposited*). Zn^{2+} , Fe^{2+} and Ni^{2+}
417 have already been found in isomorphic structure of boussingaultite replacing Mg^{2+} : katerinopoulosite
418 $(NH_4)_2[Zn(H_2O)_6](SO_4)_2$, mohrite $(NH_4)_2[Fe(H_2O)_6](SO_4)_2$, and nickelboussingaultite
419 $(NH_4)_2[Ni(H_2O)_6](SO_4)_2$. However, a Mn^{2+} member was not reported so far.

420 The structure model obtained in this study is consistent with the Raman and IR spectra of
421 boussingaultite reported and interpreted by Culka et al. (2009), collected from a sample from
422 Larderello, Tuscany, Italy (of which the chemical composition was not reported). Micro-Raman
423 (un-oriented crystal) and IR (by diffuse reflectance infrared Fourier transform – DRIFT; powder
424 mixed with KBr, in a ratio 1:10) spectra were described considering four main regions. The region
425 with the highest wavenumber (*i.e.*, above 2600 cm^{-1}) displays the combination of the OH and NH_4
426 stretching vibrations. The region between 1800 and 1400 cm^{-1} contains the spectral signals of the
427 NH_4 and HOH bending vibrations. The region between 1300 and 900 cm^{-1} contains the SO_4
428 stretching vibrations. SO_4 bending vibrations, along with the lattice modes, occur in the spectral
429 region below 800 cm^{-1} . The assignment to each Raman and infrared bands, obtained after a
430 deconvolution of combined signals, was proposed by the authors (Culka et al. 2009). Concerning
431 the region of the OH and NH_4 stretching vibrations, both Raman and DRIFT spectra provide only
432 broad bands. The deconvolution of the Raman spectrum produced a reasonable fit with four
433 independent modes assigned to OH (*i.e.*, 3380_w , 3290_w , 3080_m , and 3040_m cm^{-1}) and two
434 independent modes assigned to NH_4 (*i.e.*, 2919_w and 2845_w cm^{-1}). However, the peaks show
435 different full-width-at-half-maximum (FWHM), suggesting that additional signals were likely
436 missed (in particular at wavenumber $> 3200\text{ cm}^{-1}$). In the same region, the DRIFT spectrum show

437 only a very broad band and its deconvolution led to four independent modes, two assigned to OH
438 (*i.e.*, 3290_s and 3084_s cm⁻¹) and two to NH₄ (*i.e.*, 2913_m and 2848_m cm⁻¹). Even in this case, the
439 occurrence of more (independent and missing) signals is highly likely. A further study, based on IR
440 and Raman spectroscopy, was conducted on synthetic (NH₄)₂[Mg(H₂O)₆](SO₄)₂ by Jayakumar et al.
441 (1988), who reported the IR and polarized Raman spectra of the compound, with a careful
442 assignment of the active modes coupled with a comparative analysis on what previously observed
443 from the isomorphous K₂[Mg(H₂O)₆](SO₄)₂. Evidence of (coexisting) three different H₂O molecules
444 were reported, with relative stretching and bending vibrations. The potential $O_{\text{donor}}-H\dots O_{\text{acceptor}}$
445 distances were also deduced: ranging between 0.274-0.282 Å, in good agreement with the
446 experimental findings of this study. On the basis of the vibrational modes ascribable to the SO₄
447 group, the linear distortion of the tetrahedron (expressed by different *S-O* bonds) was found to be
448 greater than its angular distortion (expressed by different *O-S-O* angles). Conversely, the NH₄
449 tetrahedron was found to be affected by a more pronounced angular distortion, and the possibility of
450 free rotation of the NH₄ ion was ruled out. Even these last findings pertaining to the SO₄ and NH₄
451 groups are fully supported by the results of our study.

452 We expect that the experimental findings of this study, with a full description of the H-
453 bonding network in boussingaultite structure, along with the libration regime and orientation of all
454 the atomic sites (including the H sites), could lead to a better modelling of its physical and chemical
455 stability (*i.e.*, chemical reactivity in solution, phase stability under non-ambient *P/T* conditions and
456 deformation mechanisms at the atomic scale). The full understanding of the natural occurrence of
457 boussingaultite, and of its transformation paths in natural or industrial processes, requires the
458 knowledge of its physical and chemical stability. In addition, this study shed new light on the
459 mechanisms that could promote solid solution along the join boussingaultite-picromerite, and to
460 more complex (and coexisting) substitutions in the crystalline edifice $A^+_2B^{2+}(SO_4)_2(H_2O)_6$ at the *A*
461 (*e.g.*, K⁺ vs. NH₄⁺) and at the *B* (*e.g.*, Mn²⁺ vs. Mg²⁺) sites.

462

463 **Acknowledgements**

464 The authors thank the Institut Laue-Langevin (Grenoble, France) for the allocation of the beamtime.
465 GDG acknowledge the support of the Italian Ministry of Education (MIUR) through the projects
466 'Dipartimenti di Eccellenza 2018-2022' and 'PRIN2017 - Mineral reactivity, a key to understand
467 large-scale processes'. The Associate Editor, O. Tschauer, the Technical Editor team and an
468 anonymous reviewer are thanked for the revision of the manuscript.

469

470

471

472 **References**
473

474 Busing, W.R. and Levy, H.A. (1964) The effect of thermal motion on the estimation of bond
475 lengths from diffraction measurements. *Acta Crystallographica*, 17, 142-146.

476 Bosi, F., Belardi, G., and Ballirano, P. (2009) Structural features in Tutton's salts
477 $K_2[M^{2+}(H_2O)_6](SO_4)_2$, with $M^{2+} = Mg, Fe, Co, Ni, Cu,$ and Zn . *American Mineralogist*, 94, 74-82.

478 Cipriani, C. (1958) Ricerche sulla Boussingaultite manganesifera di Larderello. *Rendiconti*
479 *della Società Italiana di Mineralogia e Petrologia*, 14, 124.

480 Culka, A., Jehlička, J., and Němec, I. (2009) Raman and infrared spectroscopic study of
481 boussingaultite and nickelboussingaultite. *Spectrochimica Acta Part A: Molecular and*
482 *Biomolecular Spectroscopy*, 73, 420-423.

483 Duisenberg, A.J.M. (1992) Indexing in single-crystal diffractometry with an obstinate list of
484 reflections. *Journal of Applied Crystallography*, 25, 92-96.

485 Ende, M., Effenberger, H., Fehér, B., Sajó, I., Kótai, L., and Szakáll, S. (2021) Kollerite,
486 $(NH_4)_2Fe^{3+}(SO_3)_2(OH) \cdot H_2O$, a new sulfite mineral. *Mitteilungen der Österreichischen*
487 *Mineralogischen Gesellschaft*, 167, 88.

488 F.A.O. (2019) World fertilizer trends and outlook to 2022. Food and Agriculture Organization
489 of the United Nations, Rome (Italy). ISBN 978-92-5-131894-2.

490 Gatta, G.D., McIntyre, G.J., Sassi, R., Rotiroti, N., and Pavese, A. (2011) Hydrogen-bond and
491 cation partitioning in $2M_1$ -muscovite: A single-crystal neutron-diffraction study at 295 and 20 K.
492 *American Mineralogist*, 96, 34-41.

493 Gatta, G.D., McIntyre, G.J., Swanson, G.J., and Jacobsen, S.D. (2012) Minerals in cement
494 chemistry: a single-crystal neutron diffraction and Raman spectroscopic study of thaumasite,
495 $Ca_3Si(OH)_6(CO_3)(SO_4) \cdot 12H_2O$. *American Mineralogist*, 197, 1060-1069.

496 Gatta, G.D., Merlini, M., Valdrè, G., Liermann, H-P., Nénert, G., Rothkirch, A., Kahlenberg,
497 V., and Pavese, A. (2013) On the crystal structure and compressional behaviour of talc: a mineral of
498 interest in petrology and material science. *Physics and Chemistry of Minerals*, 40, 145-156.

499 Gatta, G.D., Nénert, G., Guastella, G., Lotti, P., Guastoni, A., and Rizzato, S. (2014) A
500 single-crystal neutron and X-ray diffraction study of a Li,Be-bearing brittle mica. *Mineralogical*
501 *Magazine*, 78, 55-72.

502 Gatta, G.D., Hålenius, U., Bosi, F., Cañadillas-Delgado, L., and Fernandez-Diaz, M.T. (2019)
503 Minerals in cement chemistry: A single-crystal neutron diffraction study of ettringite,
504 $Ca_6Al_2(SO_4)_3(OH)_{12} \cdot 27H_2O$. *American Mineralogist*, 104, 73-78.

- 505 Gatta, G.D., Guastoni, A., Lotti, P., Guastella, G., Fabelo, O., and Fernandez-Diaz, M.T.
506 (2019) A multi-methodological study of kurnakovite: A potential B-rich aggregate. American
507 Mineralogist, 104, 1315-1322.
- 508 Gatta, G.D., Guastoni, A., Lotti, P., Guastella, G., Fabelo, O., and Fernandez-Diaz, M.T.
509 (2020) A multi-methodological study of kernite, a mineral commodity of boron. American
510 Mineralogist, 105, 1424–1431.
- 511 Gatta, G.D., Comboni, D., Fernandez-Diaz, M.T. and Fabelo Rosa, O.R. (2021a) On the
512 labyrinthine world of natural borates: H-bonding network in probertite, $\text{NaCaB}_5\text{O}_7(\text{OH})_4 \cdot 3\text{H}_2\text{O}$;
513 Institut Laue-Langevin (ILL), Grenoble, 2021 (DOI: 10.5291/ILL-DATA.5-11-447).
- 514 Gatta, G.D., Hradil, K., and Meven, M. (2021b) Where is the hydrogen? Elements, 17, 163-
515 168.
- 516 Gronvold, F. and Meisingset, K.K. (1982) Thermodynamic properties and phase transitions of
517 salt hydrates between 270 and 400 K I. $\text{NH}_4\text{Al}(\text{SO}_4)_2 \cdot 12\text{H}_2\text{O}$, $\text{KAl}(\text{SO}_4)_2 \cdot 12\text{H}_2\text{O}$, $\text{Al}_2(\text{SO}_4)_3 \cdot 17\text{H}_2\text{O}$,
518 $\text{ZnSO}_4 \cdot 7\text{H}_2\text{O}$, $\text{Na}_2\text{SO}_4 \cdot 10\text{H}_2\text{O}$, and $\text{Na}_2\text{S}_2\text{O}_3 \cdot 5\text{H}_2\text{O}$. Journal of Chemical Thermodynamics, 14,
519 1083-1098.
- 520 Highfield, J., Lim, H., Fagerlund, J., and Zevenhoven, R. (2012) Activation of serpentine for
521 CO_2 mineralization by flux extraction of soluble magnesium salts using ammonium sulfate. Royal
522 Society of Chemistry Advances, 2, 6535.
- 523 Hofmann, W. (1931) Die Struktur der Tuttonschen Salze. Zeitschrift für Kristallographie,
524 Mineralogie und Petrographie, 78, 279-333.
- 525 Jayakumar, V.S., Sekar, G., Rajagopal, P., and Aruldas, G. (1988) IR and polarized Raman
526 spectra of $(\text{NH}_4)_2\text{Mg}(\text{SO}_4)_2 \cdot 6\text{H}_2\text{O}$. Physica Status Solidi, 109, 635-640.
- 527 Larson, A.C. (1967) Inclusion of secondary extinction in least-squares calculations. Acta
528 Crystallographica, 23, 664-665.
- 529 Larsen, E.S. and Shannon, E.V. (1920) Boussingaultite from South Mountain, near Santa
530 Paula, California. American Mineralogist, 5, 127-128.
- 531 Li, C., Chen, X., Guo, H., Zhou, X., and Cao, J. (2020) Production of potash and N-Mg
532 compound fertilizer via mineral shoenite from Kun Te Yi Salt Lake: Phase diagrams of the quaternary
533 system $(\text{NH}_4)_2\text{SO}_4\text{-MgSO}_4\text{-K}_2\text{SO}_4\text{-H}_2\text{O}$ in the isothermal evaporation and crystallization process. Acta
534 Geologica Sinica, 95, 1016-1023.
- 535 Lim, A.R. (2012) Thermodynamic properties and phase transitions of Tutton salt
536 $(\text{NH}_4)_2\text{Co}(\text{SO}_4)_2 \cdot 6\text{H}_2\text{O}$ crystals. Journal of Thermal Analysis and Calorimetry, 109, 1619–1623.

537 Lim, A.R. and Lee, J.H. (2010) ^{23}Na and ^{87}Rb relaxation study of the structural phase
538 transitions in the Tutton salts $\text{Na}_2\text{Zn}(\text{SO}_4)_2 \cdot 6\text{H}_2\text{O}$ and $\text{Rb}_2\text{Zn}(\text{SO}_4)_2 \cdot 6\text{H}_2\text{O}$ single crystals. *Physica*
539 *Status Solidi*, B247, 1242 - 1246.

540 Lotti, P., Gatta, G.D., Demitri, N., Guastella, G., Rizzato, S., Ortenzi, M.A., Magrini, F.,
541 Comboni, D., Guastoni, A., and Fernandez-Diaz M.T. (2018) Crystal-chemistry and temperature
542 behavior of the natural hydrous borate colemanite, a mineral commodity of boron. *Physics and*
543 *Chemistry of Minerals*, 45, 405–422.

544 Matthewman, J.C., Thompson, P., and Brown, P.J. (1982) The Cambridge crystallography
545 subroutine library. *Journal of Applied Crystallography*, 15, 167–173.

546 Margulis, T.N. and Templeton, D.H. (1962) Crystal structure and hydrogen bonding of
547 magnesium ammonium sulfate hexahydrate. *Zeitschrift für Kristallographie*, 117, 344-357.

548 Maslen, E.N., Ridout, S.C., Watson, K.J., and Moore, F.H. (1988) The structures of Tutton's
549 salts. I. Diammonium hexaaquamagnesium(II) sulfate. *Acta Crystallographica*, C44, 409-412.

550 McIntyre, G.J. and Stansfield, R.F.D. (1988) A general Lorentz correction for single-crystal
551 diffractometers. *Acta Crystallographica*, A44, 257-262.

552 Montgomery, H. and Lingafelter, E.C. (1964) The crystal structure of Tutton's salts. II.
553 Magnesium ammonium sulfate hexahydrate and nickel ammonium sulfate hexahydrate. *Acta*
554 *Crystallographica*, 17, 1478-1479.

555 Park, S.S. and Lim, A.R. (2017) Role of NH_4 and H_2O in Tutton salt $(\text{NH}_4)_2\text{M}(\text{SO}_4)_2 \cdot 6\text{H}_2\text{O}$
556 ($M=\text{Fe}$ and Zn) single crystals studied by ^1H and ^{14}N NMR at high temperatures. *Journal of the*
557 *Korean Magnetic Resonance Society*, 21, 67-71.

558 Sears, V.F. (1986) Neutron Scattering Lengths and Cross-Sections. In K. Sköld and D.L.
559 Price, Eds., *Neutron Scattering, Methods of Experimental Physics*, Vol. 23A, Academic Press, New
560 York, pp. 521-550.

561 Sheldrick, G.M. (2015) Crystal structure refinement with SHELXL. *Acta Crystallographica*
562 *Section C: Structural Chemistry*, 71, 3-8.

563 Shimobayashi, N., Ohnishi, M., and Miura, H. (2011) Ammonium sulfate minerals from
564 Mikasa, Hokkaido, Japan: boussingaultite, godovikovite, efremovite and tschermigite. *Journal of*
565 *Mineralogical and Petrological Sciences*, 1103260174-1103260174.

566 Szabó, D., Lovász, A., Weiszbürg, T., Szakáll, S., and Kristály, F. (2015) Ammonioalunite
567 and adranosite-Al. New mineral species from the burning coal dumps of Pécs-Vasas, Hungary.
568 *Proceedings of the "6th Mineral Sciences in the Carpathians Conference"*, Veszprém, Hungary, 17-
569 19 May, 2015.

570 Szakáll, S. and Kristály, F. (2008) Ammonium sulphates from burning coal dumps at Komló
571 and Pécs-Vasas, Mecsek Mts., South Hungary. Proceedings of the “2nd Central-European
572 Mineralogical Conference (CEMS)”, published in “Mineralogia, Special Papers”, 32, 154.

573 Szakáll, S., Sajó, I., Fehér, B., and Bigi, S. (2012) Ammoniomagnesiovoltaite, a new
574 voltaite-related mineral species from Pécs-Vasas, Hungary. Canadian Mineralogist, 50, 65-72.

575 Steiner, T. (1998) Opening and narrowing of the water H-O-H angle by hydrogen-bonding
576 effects: Re-inspection of neutron diffraction data. Acta Crystallographica, B54, 464-470.

577 Taweepreda, W. (2013) Rubber recovery from centrifuged natural rubber latex residue
578 using sulfuric acid. Songklanakarin Journal of Science and Technology, 35, 213-216.

579 Tutton, A.E.H. (1900) A comparative crystallographical study of the double selenates of the
580 series $R_2M(\text{SeO}_4)_2 \cdot 6\text{H}_2\text{O}$. Salts in which M is zinc. Proceedings of the Royal Society of London,
581 67(435–441), 58–84.

582 Tutton, A.E.H. (1905) The relation of ammonium to the alkali metals. A study of ammonium
583 magnesium and ammonium zinc sulphates and selenates. Journal of the Chemical Society, 87, 1123-
584 1183.

585 Wilkinson, C., Khamis, H.W., Stansfield, R.F.D., and McIntyre, G.J. (1988) Integration of
586 single-crystal reflections using area multidetectors. Journal of Applied Crystallography, 21, 471-478.

587

588

589

590

591

592

593 Table 1. REE (+Th, U) concentration by ICP-AES (see text for details).

594

	%m/m	ICP-AES (nm)	LOD	LOQ	
595	Ce ₂ O ₃	< LOD	413.764	0.003	0.01
	Dy ₂ O ₃	0.003	353.170	0.0001	0.0003
596	Er ₂ O ₃	< LOD	369.265	0.002	0.007
	Eu ₂ O ₃	< LOD	381.967	0.0001	0.0003
597	Gd ₂ O ₃	0.004	342.247	0.0003	0.001
	Ho ₂ O ₃	< LOD	345.600	0.0001	0.0003
598	La ₂ O ₃	< LOD	398.852	0.0001	0.0003
	La ₂ O ₃	< LOD	408.672	0.0002	0.0006
599	Lu ₂ O ₃	< LOD	261.542	0.0002	0.0006
600	Nd ₂ O ₃	< LOD	406.109	0.0002	0.0006
	Pr ₂ O ₃	< LOD	390.844	0.0002	0.0006
601	Sm ₂ O ₃	< LOD	359.260	0.0005	0.002
	Sc ₂ O ₃	< LOD	361.383	0.0005	0.002
602	Tb ₂ O ₃	< LOD	350.917	0.0005	0.002
	Tm ₂ O ₃	< LOD	313.126	0.004	0.015
603	Yb ₂ O ₃	< LOD	328.937	0.0001	0.0003
	Y ₂ O ₃	< LOD	371.029	0.0001	0.0003
604	ThO ₂	< LOD	283.730	0.001	0.004
605	UO ₂	< LOD	385.958	0.01	0.04

Note: LOD: Limit of detection (3σ); LOQ: Limit of quantification (10σ)

606

607

608

609 Table 2. Concentration of other minor elements by ICP-AES (see text for details).

610

	%m/m	ICP-AES (nm)		%m/m	ICP-AES (nm)	
611	Li ₂ O	< 0.01	670.784	NiO	< 0.01	231.604
	MgO	< 0.01	285.213	CuO	< 0.01	327.393
612	K ₂ O	2.92	766.490	Ag ₂ O	< 0.01	328.068
	Rb ₂ O	0.05	780.023	ZnO	< 0.01	206.200
613	Cs ₂ O	< 0.02	852.1*	CdO	< 0.01	228.802
	BeO	< 0.01	313.107	Al ₂ O ₃	< 0.02	396.153
614	CaO	< 0.01	317.933	Tl ₂ O	< 0.02	190.801
	BaO	< 0.02	233.527	PbO	< 0.05	220.353
615	TiO ₂	< 0.01	334.940	P ₂ O ₅	< 0.02	213.617
	ZrO ₂	< 0.01	343.823	As ₂ O ₃	< 0.02	193.696
616	V ₂ O ₅	< 0.02	292.464	Sb ₂ O ₃	< 0.02	206.836
	Cr ₂ O ₃	< 0.01	267.716	Bi ₂ O ₃	< 0.02	223.061
617	MoO ₃	< 0.02	202.031	SiO ₂	0.04	251.611
	MnO	1.18	257.610	SrO	< 0.01	407.771
618	Fe ₂ O ₃	0.01	238.204	B ₂ O ₃	< 0.05	249.677
	CoO	< 0.01	228.616	MgO	10.2(7)**	285.213

* by FAES; **by EDTA titration.

619 Table 3. Representative chemical composition of boussingaultite from Pécs-Vasas, and empirical
 620 formula recalculated on the basis of five cations.
 621
 622

<i>Oxides</i>	<i>Wt%</i>	<i>e.s.d.</i>
SO ₃	44.20	± 0.20
MgO	10.60	± 0.20
(NH ₄) ₂ O	12.70	± 0.30
K ₂ O	2.92	± 0.10
MnO	1.18	± 0.10
H ₂ O	28.40	± 0.20
TOTAL	100.1	

<i>Elements</i>	<i>a.p.f.u.</i>
S ⁶⁺	1.99
Mg ²⁺	0.95
NH ₄ ⁺	1.77
K ⁺	0.22
Mn ²⁺	0.06
H ⁺	11.40

Empirical formula:
 [(NH₄)_{1.77}K_{0.22}]_{Σ1.99}[(Mg_{0.95}Mn_{0.06})_{Σ1.01}(H₂O)_{5.7}](SO₄)_{1.99}
 Ideal formula:
 (NH₄)₂[Mg(H₂O)₆](SO₄)₂

631
 632
 633
 634
 635
 636
 637
 638
 639
 640
 641
 642
 643
 644
 645
 646
 647
 648
 649
 650
 651
 652
 653
 654
 655
 656
 657
 658
 659
 660
 661
 662

663
 664 Table 4 (*deposited*). Details of neutron data collections and refinements of boussingaultite. Ref.#1
 665 and Ref.#2 are referred, respectively, to the refinement *without* the *O1A* and *O2A* sites and *with* the
 666 *O1A* and *O2A* sites.

667

668

669

670

671

672

673

674

675

676

677

678

679

680

681

682

683

684

685

686

687

	Ref. #1	Ref. #2
<i>T</i> (K)	20(1)	
Crystal shape	Prism	
Crystal volume (mm)	3.5 x 2.1 x 1.6	
Crystal colour	Whitish	
Unit-cell parameters	<i>a</i> = 9.2173(1) Å <i>b</i> = 12.4215(3) Å <i>c</i> = 6.2556(2) Å β = 106.750(1)° <i>V</i> = 685.83(3) Å ³	
Reference chemical formula	(NH ₄) ₂ [Mg(H ₂ O) ₆](SO ₄) ₂	
Space Group	<i>P</i> 2 ₁ / <i>a</i>	
<i>Z</i>	2	
Radiation type, λ (Å)	Neutron CW, 0.9500	
Diffractometer	D19 four-circle - ILL	
Data-collection method	ω -scans	
<i>d</i> _{min.} (Å)	0.54	
	-14 ≤ <i>h</i> ≤ +16	
	-17 ≤ <i>k</i> ≤ +21	
	-11 ≤ <i>l</i> ≤ +5	
Measured reflections	8652	
Unique reflections	3788	
Unique reflections with <i>F</i> _o > 4σ(<i>F</i> _o)	3466	
Refined parameters	179	190
<i>R</i> _{int}	0.0371	0.0371
<i>R</i> _σ	0.0271	0.0271
<i>R</i> ₁ (<i>F</i>) with <i>F</i> _o > 4σ(<i>F</i> _o)	0.0456	0.0334
<i>R</i> ₁ (<i>F</i>) for all reflections	0.0503	0.0377
<i>wR</i> ₂ (<i>F</i> ²)	0.1132	0.0801
GooF	1.614	1.143
Residuals (fm/Å ³)	-1.93/+4.28	-1.32/+0.81

Note: Statistical parameters according to the SHELXL-2018/3 definition. The two refinements were conducted using the same weighting scheme.

688 Table 5 (*deposited*). Refined fractional atomic coordinates and equivalent/isotropic displacement
 689 factors (\AA^2) of boussingaultite, based on the neutron structure refinement at 20 K. U_{eq} is defined as
 690 one third of the trace of the orthogonalised U_{ij} tensor. *Ref.#1* and *Ref.#2* are referred, respectively, to
 691 the refinement *without* the *O1A* and *O2A* sites and *with* the *O1A* and *O2A* sites.
 692
 693

Site	Ref.#1					Ref.#2				
	s.o.f.	x/a	y/b	z/c	U_{eq}	s.o.f.	x/a	y/b	z/c	U_{eq}/U_{iso}
Mg	Mg 0.963(5), Mn 0.037(5)	0	0	0	0.0063(2)	Mg 0.947(3), Mn 0.053(3)	0	0	0	0.0063(2)
S	1	0.41004(11)	0.13300(9)	0.73463(17)	0.0058(2)	1	0.41004(8)	0.13306(7)	0.73458(12)	0.0065(1)
O1	1	0.41640(7)	0.22412(5)	0.58366(10)	0.0101(1)	0.915(6)	0.41709(10)	0.22386(5)	0.58379(7)	0.0085(2)
O1A	0					0.085(6)	0.3757(12)	0.2398(6)	0.5818(9)	0.0089(13)
O2	1	0.55141(7)	0.07043(6)	0.78275(11)	0.0126(1)	0.895(9)	0.55135(5)	0.06933(12)	0.7843(2)	0.0103(2)
O2A	0					0.105(9)	0.5519(6)	0.0945(10)	0.7497(13)	0.0095(11)
O3	1	0.28086(6)	0.06251(5)	0.61882(9)	0.00698(9)	1	0.28085(4)	0.06253(3)	0.61881(6)	0.00771(7)
O4	1	0.38669(6)	0.17482(5)	0.94525(9)	0.00811(9)	1	0.38673(5)	0.17483(4)	0.94519(6)	0.00886(7)
O5	1	0.17381(6)	0.10514(5)	0.16477(9)	0.00817(9)	1	0.17383(4)	0.10513(4)	0.16480(6)	0.00892(7)
O6	1	-0.16162(6)	0.11309(5)	0.02944(9)	0.00788(9)	1	-0.16161(4)	0.11310(4)	0.02949(7)	0.00865(7)
O7	1	-0.00322(6)	-0.06902(5)	0.29772(9)	0.00767(9)	1	-0.00322(4)	-0.06900(4)	0.29778(6)	0.00833(7)
N	1	0.13458(4)	0.34231(4)	0.35306(6)	0.01071(7)	N 0.869(3), K 0.131(3)	0.13458(3)	0.34233(3)	0.35303(4)	0.00939(6)
H1	1	0.0679(2)	0.32960(18)	0.1934(3)	0.0323(4)	0.869(3)	0.06782(16)	0.32964(13)	0.1932(2)	0.0285(3)
H2	1	0.2283(2)	0.29287(17)	0.3925(4)	0.0311(3)	0.869(3)	0.22826(14)	0.29285(12)	0.3925(3)	0.0274(2)
H3	1	0.0689(2)	0.32369(19)	0.4569(3)	0.0327(4)	0.869(3)	0.06905(16)	0.32356(14)	0.4569(2)	0.0288(3)
H4	1	0.1681(2)	0.42188(15)	0.3706(3)	0.0301(3)	0.869(3)	0.16799(16)	0.42181(11)	0.3707(2)	0.0266(2)
H5	1	0.22321(17)	0.08793(14)	0.3220(2)	0.0228(2)	1	0.22316(12)	0.08793(10)	0.32201(15)	0.0235(2)
H6	1	0.25245(16)	0.12143(14)	0.0937(2)	0.0234(2)	1	0.25241(12)	0.12140(10)	0.09347(18)	0.0242(2)
H7	1	-0.26636(14)	0.09873(13)	-0.0587(2)	0.0209(2)	1	-0.26636(10)	0.09870(9)	-0.05881(17)	0.0218(2)
H8	1	-0.14189(17)	0.18806(12)	-0.0019(3)	0.0219(2)	1	-0.14187(12)	0.18804(9)	-0.00188(18)	0.0227(2)
H9	1	-0.09577(17)	-0.05940(14)	0.3425(3)	0.0233(2)	1	-0.09572(12)	-0.05947(10)	0.34248(19)	0.0242(2)
H10	1	0.02592(17)	-0.14424(12)	0.3301(2)	0.0217(2)	1	0.02595(12)	-0.14428(9)	0.33009(18)	0.0226(2)

*s.o.f.(O1)+s.o.f.(O1A) = 1, s.o.f.(O2)+s.o.f.(O2A) = 1, s.o.f.(N) = s.o.f.(H1,..., H4),
 O1A and O2A were modelled as isotropic*

694
 695
 696
 697
 698
 699
 700

701
702
703
704
705
706

Table 6 (*deposited*). Refined displacement parameters (\AA^2) of boussingaultite in the expression: $-2\pi^2[(ha^*)^2U_{11} + \dots + 2hka^*b^*U_{12} + \dots + 2klb^*c^*U_{23}]$, based on the neutron structure refinement at 20 K. *Ref.#1* and *Ref.#2* are referred, respectively, to the refinement *without* the *O1A* and *O2A* sites and *with* the *O1A* and *O2A* sites.

Ref.#1	U_{11}	U_{22}	U_{33}	U_{23}	U_{13}	U_{12}
Mg	0.0056(3)	0.0063(4)	0.0066(3)	0.0002(2)	0.0010(2)	0.0004(2)
S	0.0041(3)	0.0057(4)	0.0070(3)	-0.0009(3)	0.0007(2)	-0.0009(3)
O1	0.0127(2)	0.0076(2)	0.0102(2)	0.0003(2)	0.0033(1)	-0.0029(2)
O2	0.0058(2)	0.0134(3)	0.0166(2)	-0.0036(2)	0.0002(2)	0.0017(2)
O3	0.0054(2)	0.0067(2)	0.0081(2)	-0.0009(1)	0.0007(1)	-0.0017(1)
O4	0.0099(2)	0.0065(2)	0.0073(2)	-0.0010(1)	0.0016(1)	-0.0002(1)
O5	0.0076(2)	0.0082(2)	0.0077(2)	0.0001(1)	0.0005(1)	-0.0016(1)
O6	0.0066(2)	0.0068(2)	0.0097(2)	0.0003(1)	0.0015(1)	0.0007(1)
O7	0.0081(2)	0.0069(2)	0.0082(2)	0.0007(1)	0.0027(1)	0.0004(1)
N	0.0101(1)	0.0111(2)	0.0110(1)	-0.0001(1)	0.0031(1)	-0.0003(1)
H1	0.0333(7)	0.0393(10)	0.0194(5)	-0.0025(5)	-0.0002(5)	-0.0069(7)
H2	0.0234(6)	0.0282(9)	0.0421(9)	0.0046(6)	0.0103(6)	0.0099(5)
H3	0.0318(7)	0.0415(10)	0.0306(7)	0.0068(6)	0.0184(6)	0.0037(7)
H4	0.0331(7)	0.0182(7)	0.0360(8)	-0.0013(5)	0.0050(6)	-0.0030(5)
H5	0.0232(5)	0.0274(7)	0.0146(4)	0.0028(4)	0.0004(4)	-0.0012(5)
H6	0.0198(5)	0.0287(7)	0.0241(5)	0.0002(5)	0.0103(4)	-0.0053(4)
H7	0.0132(4)	0.0214(6)	0.0253(5)	-0.0013(4)	0.0010(3)	-0.0016(4)
H8	0.0234(5)	0.0128(6)	0.0294(6)	0.0016(4)	0.0077(4)	-0.0020(8)
H9	0.0213(5)	0.0259(7)	0.0272(6)	0.0027(5)	0.0141(4)	0.0054(4)
H10	0.0256(5)	0.0144(6)	0.0256(5)	0.0039(4)	0.0083(4)	0.0041(4)

720

Ref.#2	U_{11}	U_{22}	U_{33}	U_{23}	U_{13}	U_{12}
Mg	0.0057(2)	0.0059(3)	0.0068(2)	0.0002(2)	0.0011(1)	0.0001(1)
S	0.0051(2)	0.0063(3)	0.0075(2)	-0.0006(2)	0.0007(2)	-0.0009(2)
O1	0.0091(3)	0.0064(2)	0.0101(2)	0.0003(1)	0.0032(1)	-0.0012(2)
O2	0.0058(2)	0.0086(4)	0.0147(3)	-0.0003(3)	0.0002(1)	0.0016(1)
O3	0.0061(1)	0.0075(2)	0.0088(1)	-0.00096(9)	0.0009(1)	-0.0016(1)
O4	0.0107(1)	0.0074(2)	0.0079(1)	-0.00095(9)	0.0017(1)	-0.0001(1)
O5	0.0082(1)	0.0090(2)	0.0084(1)	-0.0001(1)	0.0007(1)	-0.0017(1)
O6	0.0073(1)	0.0078(2)	0.0104(1)	0.0003(1)	0.0016(1)	0.0003(1)
O7	0.0088(1)	0.0075(2)	0.0089(1)	0.0008(1)	0.0028(1)	0.0004(1)
N	0.0089(1)	0.0097(1)	0.0096(1)	-0.00013(7)	0.00279(7)	-0.00037(7)
H1	0.0306(5)	0.0337(7)	0.0169(4)	-0.0021(4)	-0.0004(4)	-0.0066(5)
H2	0.0208(4)	0.0234(6)	0.0388(6)	0.0042(4)	0.0098(4)	0.0090(4)
H3	0.0285(5)	0.0363(7)	0.0270(5)	0.0060(4)	0.0166(4)	0.0030(5)
H4	0.0296(5)	0.0150(5)	0.0323(5)	-0.0012(4)	0.0042(4)	-0.0026(4)
H5	0.0238(4)	0.0285(5)	0.0150(3)	0.0029(3)	0.0005(3)	-0.0014(3)
H6	0.0207(3)	0.0295(5)	0.0248(4)	-0.0002(3)	0.0105(3)	-0.0060(3)
H7	0.0137(3)	0.0225(5)	0.0261(4)	-0.0014(3)	0.0011(2)	-0.0016(3)
H8	0.0240(4)	0.0139(4)	0.0298(4)	0.0017(3)	0.0074(3)	-0.0019(3)
H9	0.0219(3)	0.0271(5)	0.0281(4)	0.0026(3)	0.0142(3)	0.0054(3)
H10	0.0264(4)	0.0153(4)	0.0266(4)	0.0041(3)	0.0087(3)	0.0044(3)

Note: *O1A* and *O2A* were modelled as isotropic

721
722
723
724
725
726
727
728
729

730
731
732
733
734
735
736

Table 7 (*deposited*). Principal root-mean-square components (Å) of the atomic displacement parameters of the H sites, based on the neutron structure refinement at 20 K. *Ref.#1* and *Ref.#2* are referred, respectively, to the refinement *without* the *O1A* and *O2A* sites and *with* the *O1A* and *O2A* sites.

<i>Ref.#1</i>	RMS_{\min}	RMS_{mid}	RMS_{\max}	RMS_{\max}/RMS_{\min}
<i>H1</i>	0.129	0.186	0.213	1.65
<i>H2</i>	0.124	0.186	0.208	1.68
<i>H3</i>	0.132	0.183	0.216	1.63
<i>H4</i>	0.132	0.176	0.204	1.55
<i>H5</i>	0.114	0.158	0.174	1.53
<i>H6</i>	0.118	0.158	0.177	1.50
<i>H7</i>	0.111	0.147	0.170	1.53
<i>H8</i>	0.111	0.164	0.173	1.56
<i>H9</i>	0.114	0.154	0.182	1.60
<i>H10</i>	0.113	0.156	0.168	1.49
<i>Ref.#2</i>	RMS_{\min}	RMS_{mid}	RMS_{\max}	RMS_{\max}/RMS_{\min}
<i>H1</i>	0.121	0.173	0.202	1.68
<i>H2</i>	0.114	0.172	0.199	1.76
<i>H3</i>	0.124	0.173	0.203	1.64
<i>H4</i>	0.120	0.166	0.194	1.62
<i>H5</i>	0.116	0.160	0.178	1.53
<i>H6</i>	0.120	0.159	0.180	1.50
<i>H7</i>	0.113	0.151	0.172	1.52
<i>H8</i>	0.115	0.156	0.174	1.52
<i>H9</i>	0.117	0.158	0.185	1.58
<i>H10</i>	0.115	0.158	0.171	1.48

e.s.d. of RMS on the last digit

737
738
739
740
741
742
743
744
745
746
747
748
749
750
751
752
753
754
755
756
757
758
759
760
761
762

763 Table 8. Relevant bond distances (Å) and angles (°) based on the neutron structure refinement at 20
 764 K. *Ref.#1* and *Ref.#2* are referred, respectively, to the refinement *without* the *O1A* and *O2A* sites
 765 and *with* the *O1A* and *O2A* sites.
 766
 767

768	<i>Ref.#1</i>					
768	Mg-O5 (x2)	2.0936(6)	O7-Mg-O5 (x2)	88.69(2)	O5-H5	0.981(1)
769	Mg-O6 (x2)	2.0939(6)	O7-Mg-O5' (x2)	91.31(2)	O5-H5*	1.001
770	Mg-O7 (x2)	2.0582(6)	O7-Mg-O6 (x2)	89.79(2)	O5...O3	2.776(1)
771	S-O1	1.486(1)	O7-Mg-O6' (x2)	90.21(2)	H5...O3	1.806(1)
772	S-O2	1.472(1)	O5-Mg-O6 (x2)	89.94(2)	O5-H5...O3	169.4(1)
773	S-O3	1.487(1)	O5-Mg-O6' (x2)	90.06(2)	O5-H6	0.975(2)
774	S-O4	1.488(1)	O2-S-O1	109.72(8)	O5-H6*	0.995
775	N-H1	1.023(2)	O2-S-O3	109.03(8)	O5...O4	2.835(1)
776	N-H1*	1.0520	O1-S-O3	108.15(7)	H6...O4	1.870(1)
777	N...O4	2.901(1)	O2-S-O4	110.40(7)	O5-H6...O4	170.4(1)
778	H1...O4	1.925(2)	O1-S-O4	109.82(8)	H5-O5-H6	108.1(1)
779	N-H1 ...O4	158.3(1)	O3-S-O4	109.69(7)	O6-H7	0.980(1)
780	N-H2	1.030(2)	H1-N-H2	111.6(2)	O6-H7*	0.998
781	N-H2*	1.057	H1-N-H3	106.4(2)	O6...O2	2.703(1)
782	N...O1	2.971(1)	H1-N-H4	109.2(2)	H7...O2	1.723(1)
783	H2...O1	1.993(2)	H2-N-H3	108.6(2)	O6-H7...O2	178.4(1)
784	N-H2...O1	157.5(2)	H2-N-H4	109.9(2)	O6-H8	0.979(2)
785	N-H3	1.034(2)	H3-N-H4	111.0(2)	O6-H8*	0.998
786	N-H3*	1.0620			O6...O4	2.748(1)
787	N...O1	2.912(1)			H8...O4	1.769(2)
788	H3...O1	1.897(2)			O6-H8...O4	177.5(1)
789	N-H3...O1	166.2(2)			H7-O6-H8	105.7(1)
790	N-H4	1.032(2)			O7-H9	0.979(2)
791	N-H4*	1.0567			O7-H9*	1.001
792	N...O3	2.836(1)			O7...O3	2.756(1)
793	H4...O3	1.805(2)			H9...O3	1.791(2)
794	N-H4...O3	176.0(2)			O7-H9...O3	168.1(2)
795					O7-H10	0.977(2)
796					O7-H10*	0.996
797					O7...O1	2.730(1)
798					H10...O1	1.756(2)
799					O7-H10...O1	174.3(1)
800					H9-O7-H10	105.5(1)

* Bond distance corrected for "riding motion" effect, following Busing and Levy (1964)

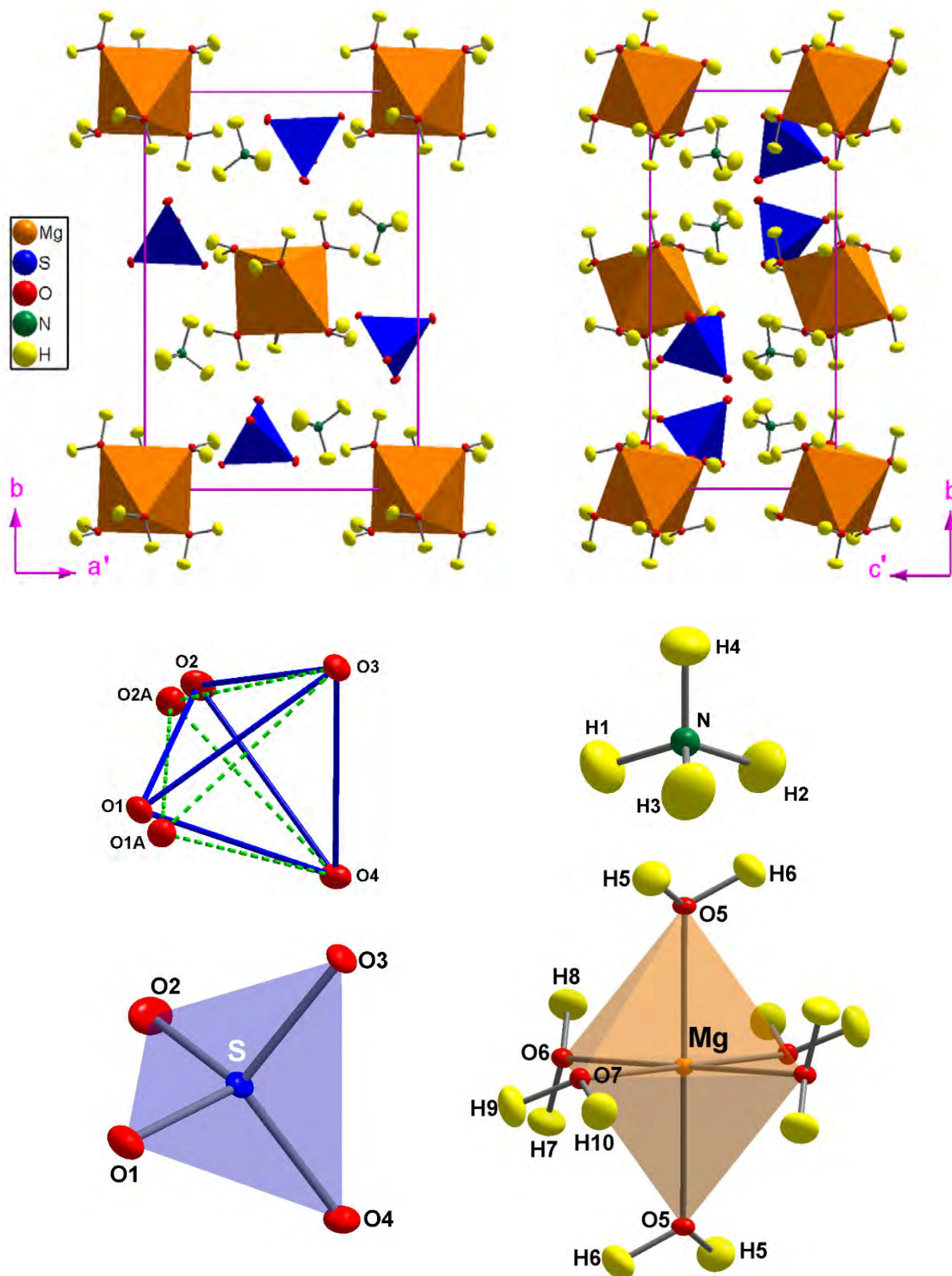
801
802
803
804
805
806
807
808
809
810

811
812
813
814
815
816
817
818
819
820
821
822
823
824
825
826
827
828
829
830
831
832
833
834
835
836
837
838
839
840
841
842
843
844
845
846
847
848
849
850
851
852
853
854
855

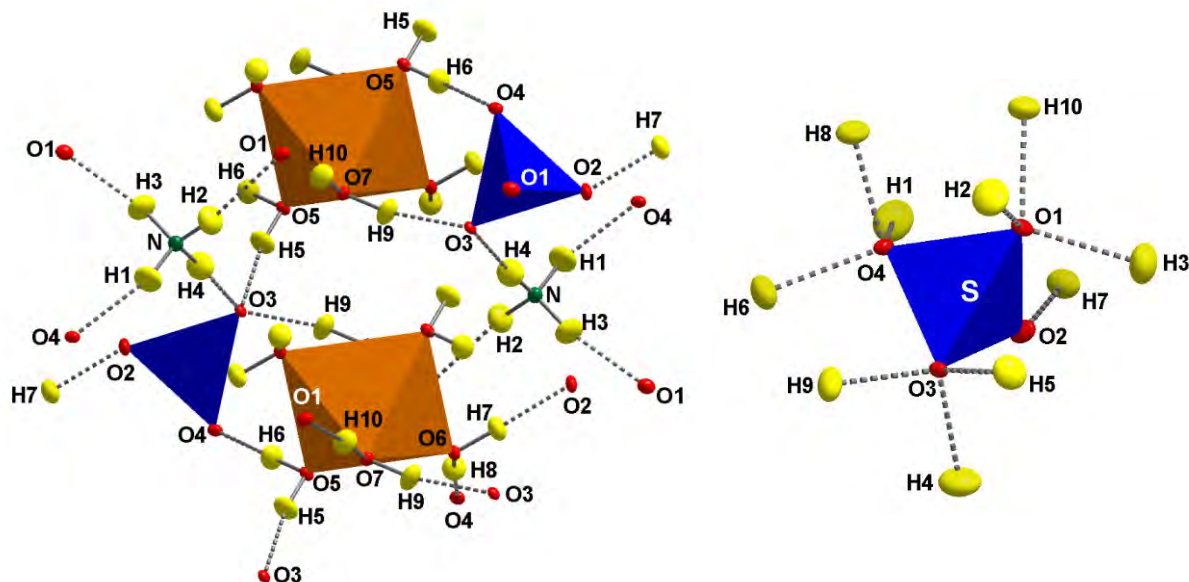
Ref.#2					
<i>Mg-O5</i> (x2)	2.0936(4)	<i>O7-Mg-O5</i> (x2)	88.70(2)	<i>O5-H5</i>	0.981(1)
<i>Mg-O6</i> (x2)	2.0941(4)	<i>O7-Mg-O5'</i> (x2)	91.30(2)	<i>O5-H5*</i>	1.001
<i>Mg-O7</i> (x2)	2.0584(4)	<i>O7-Mg-O6</i> (x2)	89.80(2)	<i>O5...O3</i>	2.776(1)
		<i>O7-Mg-O6'</i> (x2)	90.20(2)	<i>H5...O3</i>	1.806(1)
<i>S-O1</i>	1.484(1)	<i>O5-Mg-O6</i> (x2)	89.94(2)	<i>O5-H5...O3</i>	169.48(9)
<i>S-O2</i>	1.479(1)	<i>O5-Mg-O6'</i> (x2)	90.06(2)		
<i>S-O3</i>	1.488(1)			<i>O5-H6</i>	0.975(1)
<i>S-O4</i>	1.488(1)	<i>O2-S-O1</i>	110.09(9)	<i>O5-H6*</i>	0.996
[<i>S↔O1A</i>	1.612(8)]	<i>O2-S-O3</i>	108.67(7)	<i>O5...O4</i>	2.836(1)
[<i>S↔O2A</i>	1.370(6)]	<i>O1-S-O3</i>	108.29(5)	<i>H6...O4</i>	1.870(1)
		<i>O2-S-O4</i>	110.09(6)	<i>O5-H6...O4</i>	170.4(1)
<i>K-O1A</i>	2.603(1)	<i>O1-S-O4</i>	109.99(6)		
<i>K-O1A'</i>	3.279(1)	<i>O3-S-O4</i>	109.68(5)	<i>H5-O5-H6</i>	108.2(1)
<i>K-O2</i>	3.283(0)				
<i>K-O2A</i>	2.906(1)	<i>O3-O4</i>	2.433(1)	<i>O6-H7</i>	0.981(1)
<i>K-O3</i>	2.836(0)	<i>O3-O2</i>	2.410(1)	<i>O6-H7*</i>	0.998
<i>K-O4</i>	2.901(2)	<i>O2-O1</i>	2.428(1)	<i>O6...O2</i>	2.703(1)
<i>K-O5</i>	3.232(0)	<i>O1-O4</i>	2.434(1)	<i>H7...O2</i>	1.723(1)
<i>K-O6</i>	3.182(1)	<i>O4-O3-O2</i>	60.28(1)	<i>O6-H7...O2</i>	178.2(1)
		<i>O3-O2-O1</i>	59.71(1)	<i>O6...O2A</i>	2.725(5)
<i>N-H1</i>	1.024(1)	<i>O2-O1-O4</i>	60.01(1)	<i>H7...O2A</i>	1.757(5)
<i>N-H1*</i>	1.050	<i>O1-O4-O3</i>	59.32(1)	<i>O6-H7...O2A</i>	168.5(2)
<i>N...O4</i>	2.901(1)				
<i>H1...O4</i>	1.924(1)	<i>O3-O4</i>	2.433(1)	<i>O6-H8</i>	0.979(1)
<i>N-H1...O4</i>	158.3(1)	<i>O3-O2A</i>	2.427(1)	<i>O6-H8*</i>	0.998
		<i>O2A-O1A</i>	2.453(1)	<i>O6...O4</i>	2.748(1)
<i>N-H2</i>	1.030(1)	<i>O1A-O4</i>	2.387(1)	<i>H8...O4</i>	1.769(1)
<i>N-H2*</i>	1.055	<i>O4-O3-O2A</i>	59.88(2)	<i>O6-H8...O4</i>	177.5(1)
<i>N...O1</i>	2.977(1)	<i>O3-O2A-O1A</i>	59.06(2)		
<i>H2...O1</i>	1.999(1)	<i>O2A-O1A-O4</i>	60.13(2)	<i>H7-O6-H8</i>	105.7(1)
<i>N-H2...O1</i>	157.6(1)	<i>O1A-O4-O3</i>	59.87(2)		
				<i>O7-H9</i>	0.978(1)
<i>N-H3</i>	1.033(1)	<i>H1-N-H2</i>	111.6(1)	<i>O7-H9*</i>	0.999
<i>N-H3*</i>	1.058	<i>H1-N-H3</i>	106.5(1)	<i>O7...O3</i>	2.756(1)
<i>N...O1</i>	2.906(1)	<i>H1-N-H4</i>	109.2(1)	<i>H9...O3</i>	1.792(1)
<i>H3...O1</i>	1.892(2)	<i>H2-N-H3</i>	108.4(1)	<i>O7-H9...O3</i>	168.2(1)
<i>N-H3...O1</i>	166.3(1)	<i>H2-N-H4</i>	110.0(1)		
		<i>H3-N-H4</i>	111.0(1)	<i>O7-H10</i>	0.978(1)
<i>N-H4</i>	1.031(1)			<i>O7-H10*</i>	0.997
<i>N-H4*</i>	1.053			<i>O7...O1</i>	2.731(1)
<i>N...O3</i>	2.836(1)			<i>H10...O1</i>	1.757(1)
<i>H4...O3</i>	1.807(1)			<i>O7-H10...O1</i>	174.3(1)
<i>N-H4...O3</i>	175.9(1)				
				<i>H9-O7-H10</i>	105.5(1)

* Bond distance corrected for "riding motion" effect, following Busing and Levy (1964)

856 Figure 1. The crystal structure of boussingaultite, based on the neutron structure refinement of this study
857 (intensity data collected at 20 K), viewed down [001] and [100]. Configuration of the building-block units:
858 $\text{Mg}(\text{H}_2\text{O})_6$ -octahedron, SO_4 -tetrahedron and NH_4 -tetrahedron (not to scale). SO_4 -tetrahedron in response to
859 the K^+ vs. NH_4^+ substitution, with a sort of rotation of the polyhedron about the $\text{O}3\text{-O}4$ vector: the $\text{O}3$ and $\text{O}4$
860 sites are kept, whereas the $\text{O}1$ and $\text{O}2$ sites are replaced respectively by the $\text{O}1\text{A}$ and $\text{O}2\text{A}$ sites, only $\sim 0.4 \text{ \AA}$
861 from the parental ones. Displacement ellipsoid probability factor: 50%.



907 Figure 2. The complex H-bonding network into the crystal structure of boussingaultite, based on the
908 single-crystal neutron structure refinement of this study (intensity data collected at 20 K). Details in
909 Table 8. Displacement ellipsoid probability factor: 50%.



920
921
922
923
924
925
926
927
928
929
930
931
932
933
934
935
936
937
938
939
940
941
942
943
944
945
946
947
948
949
950
951
952
953
954
955
956
957
958
959
960